Supporting Information for:

# Spectral- and Structural Variations of Biomimetic Light-Harvesting Nanotubes

**A. Löhner[a†], T. Kunsel[b†], M. I .S. Röhr[c†], T. L. C. Jansen[b], S. Sengupta [c], F. Würthner[c,d*], J. Knoester[b*] and J. Köhler[a,d,e*]**

[a]*Spectroscopy of Soft Matter,*
*University of Bayreuth, Universitätsstraße 30, 94557 Bayreuth, Germany*
[b]*University of Groningen, Zernike Institute for Advanced Materials, Nijenborgh 4, 9747 AG Groningen, The Netherlands*
[c]*Universität Würzburg, Center for Nanosystems Chemistry, Theodor-Boveri-Weg, 97074 Würzburg, Germany*
[d]*Bavarian Polymer Institute,*
*Universitätsstraße 30, 94557 Bayreuth, Germany*
*Theodor-Boveri-Weg, 97074 Würzburg, Germany*
[e]*Bayreuth Institute of Macromolecular Research (BIMF), University of Bayreuth, Universitätsstraße 30, 94557 Bayreuth, Germany*

† contributed equally to this work
* corresponding authors

Contents

## 1. Further distributions of spectral parameters

### a) Lorentzian lineshapes

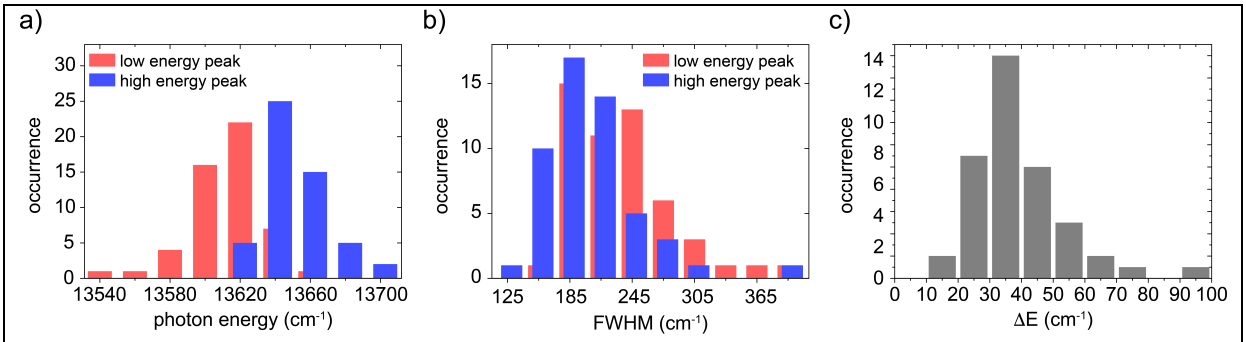


*Fig.S1: Additional parameters extracted from the polarisation-resolved spectra using Lorentzian profiles for fitting the lineshapes: a) Distributions of the spectral peak positions of the two fitted subbands (red, blue). b) Distributions of the bandwidths (FWHM) of the two subbands (red, blue). c) Distribution of the energetic separations $\Delta E$ between the two subbands*

### b) Gaussian lineshapes

In addition to the analysis for the two-component fit provided in the main text we analysed the spectra also using gaussian profiles for the lineshapes. Hence the expression for fitting the polarization-resolved spectra was modified to:

$$F(E,\theta) = B + \sum_i A_i(E)\,[\cos(\theta-\phi_i)]^2 \exp\left(-\frac{(E-E_i)^2}{W_i/2\sqrt{ln2}}\right) \qquad (S1)$$

The meaning of the parameters $B$, $A_i$, $\Theta$, and $\phi_i$ is the same as in the main text. The Gaussian form is characterized by the energetic centre position $E_i$ and a FWHM denoted by $W_i$. For the example shown in fig.1a of the main text the results of using Lorentzian or Gaussian profiles for the lineshapes are compared in table S1.

*Table S1: Fit parameters for the example aggregate shown in fig.1a of the main text, using Gaussian profiles for the lineshapes. For better comparison, the results for Lorentzian lineshapes as used in the main text are reproduced as well.*

| | Gaussian lineshape | | Lorentzian lineshape | |
|---|---|---|---|---|
| | Band 1 | Band 2 | Band 1 | Band 2 |
| $E_i$ ($cm^{-1}$) | 13598.8 | 13645.3 | 13602.3 | 13645.8 |
| $W_i$ ($cm^{-1}$) | 208.9 | 162.3 | 209.8 | 162.3 |
| $O_1/O_2$ | 1.13 | | 1.15 | |
| $\Delta\phi_{12}$ (°) | 88.8 | | 89.0 | |

For all individual ZnChl **1** nanotubes studied the corresponding distributions of the spectral parameters are presented in fig.S2, and the statistical data of the histograms are summarised in table S2.

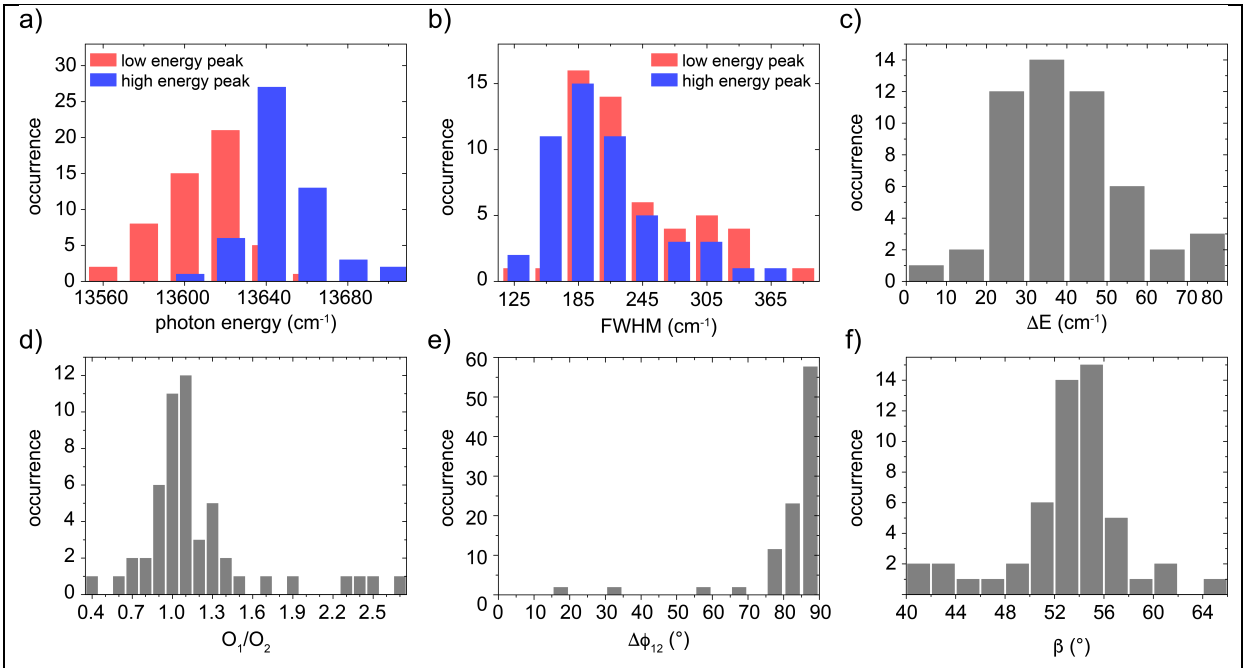


*Fig.S2: Analysis of the polarisation-resolved spectra using Gaussian profiles for fitting the lineshapes: a) Distributions of the spectral peak positions of the two fitted subbands (red, blue). b) Distributions of the bandwidths (FWHM) of the two subbands (red, blue). c) Distribution of the energetic separations ΔE between the two subbands. d) Distribution of the ratio of the oscillator strengths $O_1/O_2$ of the two subbands from an individual aggregate. e) Distribution of the relative phase angles between the two subbands from an individual aggregate. f) Distribution of the angle β that characterizes the orientation of the transition-dipole moments of the monomers with respect to symmetry axis of a tubular aggregate.*

*Table S2: Mean values and standard deviations obtained from the distributions shown in fig. S2, using Gaussian profiles for the lineshapes. For better comparison, the results for Lorentzian lineshapes as used in the main text are reproduced as well.*

| | Gaussian lineshape | | Lorentzian lineshape | |
|---|---|---|---|---|
| | Band 1 | Band 2 | Band 1 | Band 2 |
| $E_i$ ($cm^{-1}$) | 13608 ± 20 | 13647 ± 18 | 13611 ± 20 | 13649 ± 19 |
| $W_i$ ($cm^{-1}$) | 233 ± 60 | 208 ± 50 | 232 ± 48 | 207 ± 46 |
| ΔE ($cm^{-1}$) | 39 ± 15 | | 39 ± 15 | |
| $\Delta\phi_{12}$ (°) | 82 ± 13 | | 84 ± 8 | |
| $O_1/O_2$ | 1.18 ± 0.45 | | 1.23 ± 0.63 | |
| $W_1/W_2$ | 1.14 ± 0.23 | | 1.13 ± 0.15 | |
| β (°) | 53.1 ± 4.6 | | 52.8 ± 4.3 | |

c) Distribution of the fluorescence intensity

The histogram in fig.S3 shows the distribution of the integrated emitted intensity for all nano tubes studied. Next to possible variations in the number of assembled monomers, the variation of the intensity is also ascribed to slightly different excitation conditions. For example the width of the nanotubes is much smaller than the diffraction-limited focus of the laser excitation and therefore an individual tube might not always been hit perfectly in the centre. Nevertheless, for the vast majority of the aggregates (90%) the total emitted intensity reproduces within a factor of 2, reflecting a large degree of homogeneity.

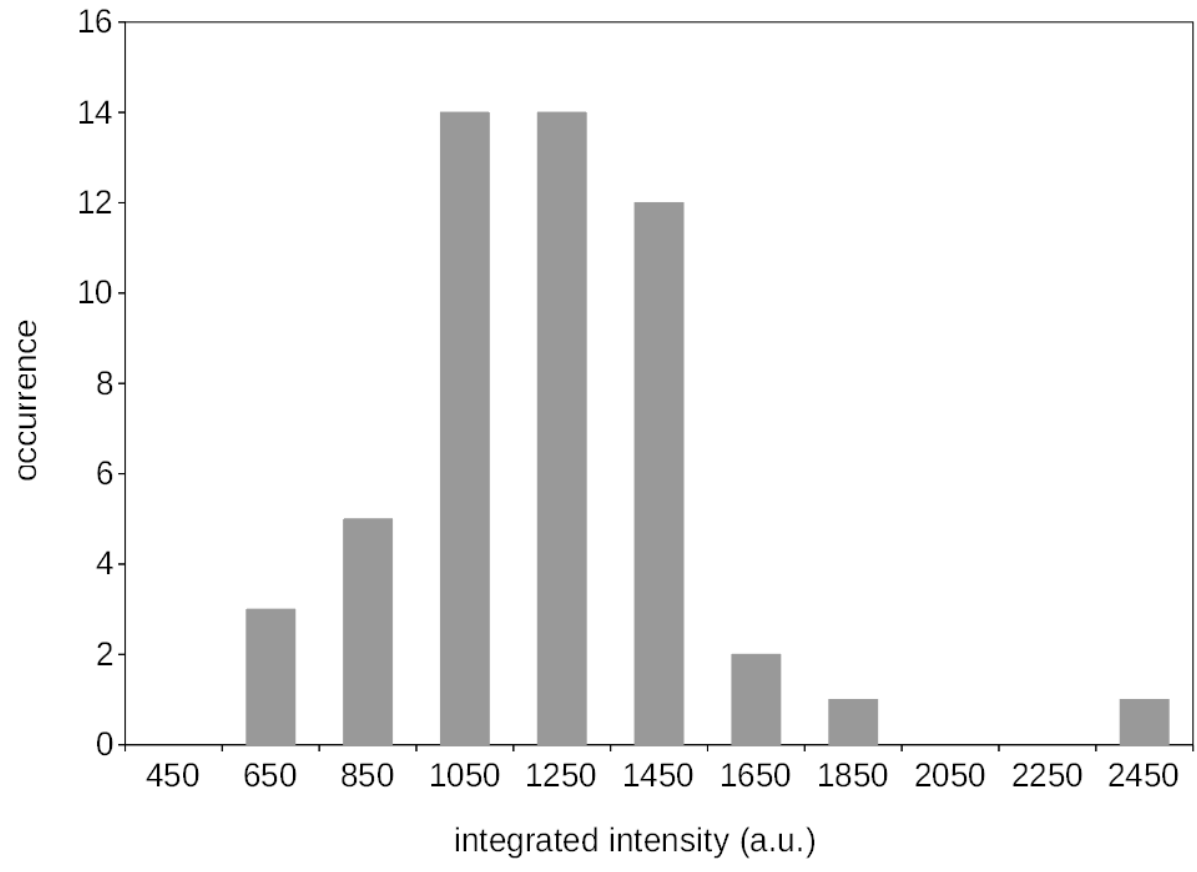


*Fig.S3: Distribution of the total polarization-averaged intensity emitted from the nanotubes. The intensity is given in arbitrary units.*

## 2. Molecular Modelling

For a systematic search of the most stable structure that fulfills the given experimental constraints, we have constructed aggregates with $N_2$ ranging from 12 to 16 and have systematically scanned the energy of a 2x2 arrangement of monomers as a function of the two undetermined parameters h and $\varphi$ employing the semiempirical PM6-D3H4 method as implemented in the MOPAC package. In this way „Ramachandran-like“ plots have been calculated from which stability regions can be identified and optimal values of the parameters h and $\varphi$ can be extracted, see fig.S4.

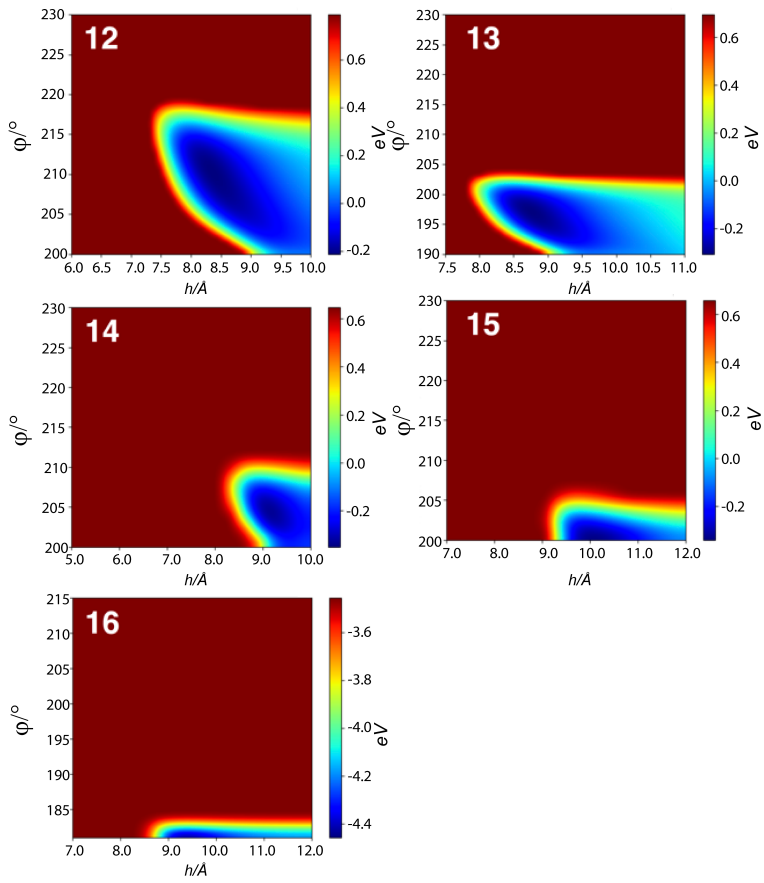


*Fig.S4: Energy scans as function of parameters h and $\varphi$ for $N_2$ ranging from 12 to 16*

From the subsequent optimization of structures corresponding to the optimal parameters extracted from the energy plots we determined that the tubular structure with $N_2$=13 is the most stable structure. We furthermore optimized an aggregate structure consisting of three-rings both by employing PM6-D3H4 as well as DFTB-D, the latter is shown in fig.S5.

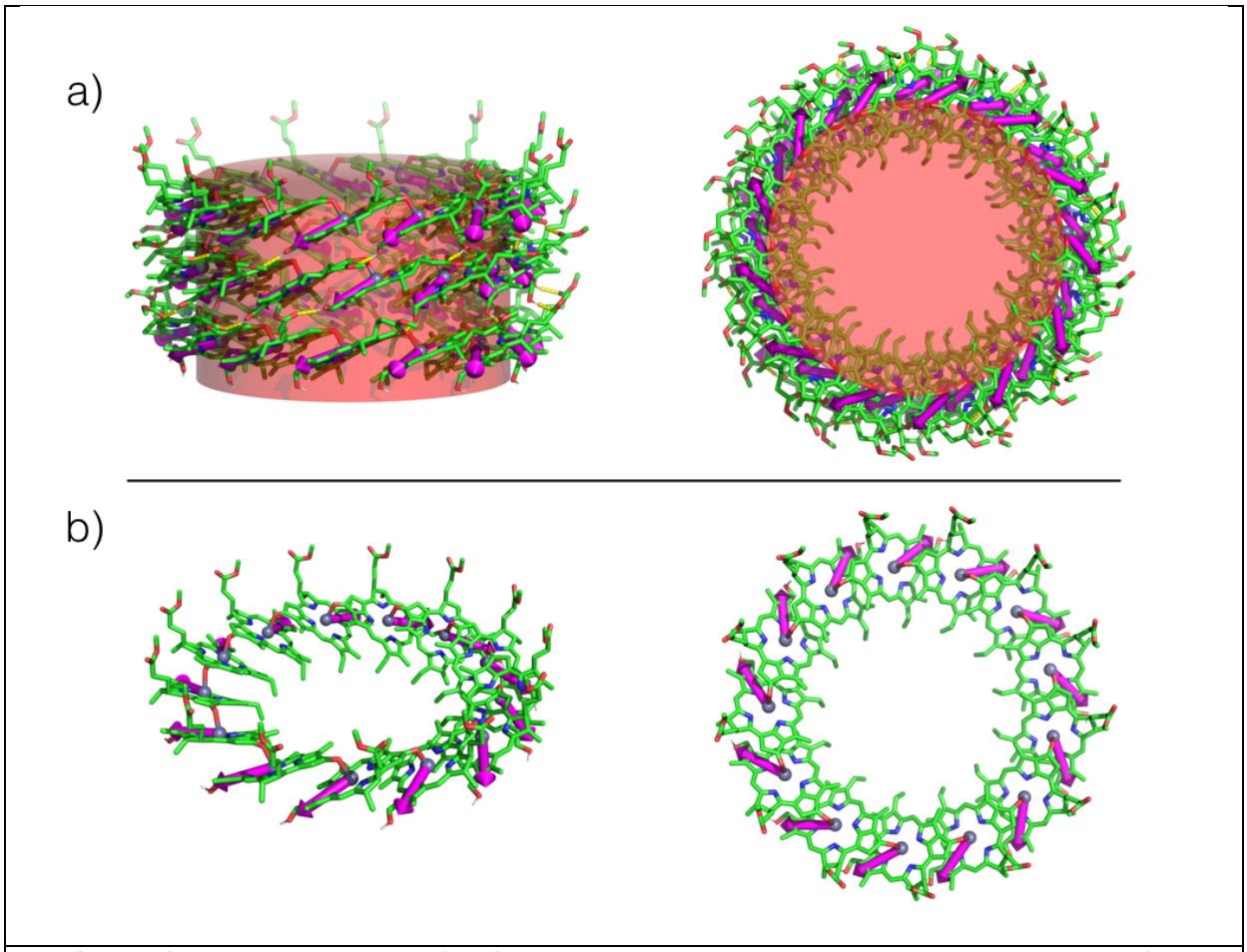


*Fig.S5 a) Side and top view of a fully optimized aggregate (DFTB-D) consisting of three rings. Transition-dipole moments are plotted as arrows, hydrogen bonds are indicated as yellow dotted lines. b) Illustration of a single ring taken from the optimized structure.*

**3. Animated movie of the optimized structure**

An animated movie of the optimized structure is provided here: link

## 4. Transition-Dipole moments and Lattice structures

In order to compare the results from the full optimization with the given experimental parameters, we plotted the transition-dipole moments of the individual monomers within the optimized “two-ring” aggregate structure along with those obtained from modelling the experimentally obtained spectral patterns for all four aggregates. The comparison is given in fig.S6 showing a good agreement.

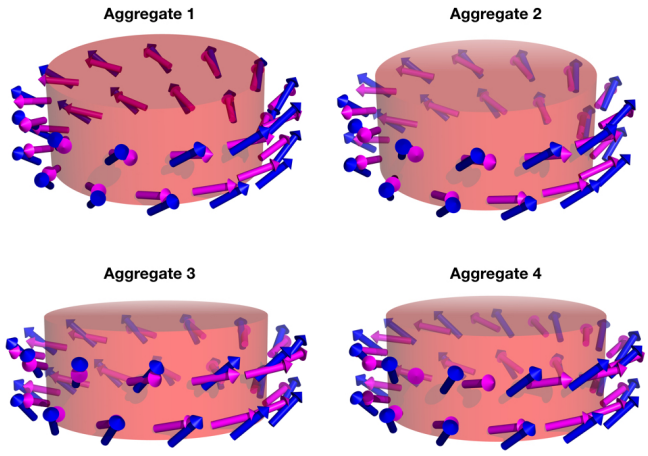


*Fig.S6: Comparison of the mutual orientation of the molecular transition-dipole moments from the optimized structure (magenta arrows) of a two ring aggregate with those obtained from simulating the experimentally observed spectral patterns (blue arrows) for all four aggregates, see also fig.4 and table 3 of the main text*

Upon wrapping onto a cylindrical surface the two-dimensional Bravais lattices shown in fig.S7 yield the tubular structures that reproduce the spectral profiles of aggregates 1-4 analyzed in the main text.

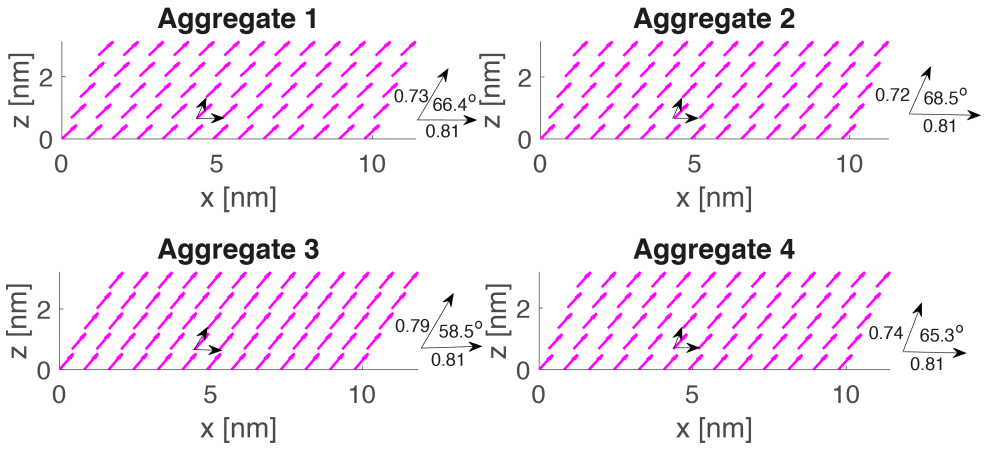


*Fig.S7: Bravais lattices underlying the tubular molecular arrangements that yield the four polarization-resolved fluorescence-excitation spectra shown in fig.4 of the main text. The magenta arrows represent the molecular transition dipole moments. The lattices have been obtained by unrolling the corresponding tubular arrangement. For each lattice the unit cell parameters are shown next to the grid.*

**5. Spectral simulation**

Since we are interested only in the $Q_y$ transition of the ZnChl **1** monomers, each molecule may be presented optically as a two–level system with a ground state and one excited state, separated by an energy $E_0 = \hbar\omega_o$. The optical transitions of different molecules are coupled by the resonance interactions between their transition dipoles, $V_{nm}$, leading to the well-known Frenkel exciton Hamiltonian:

$$H = \sum_{n,m} H_{nm}\, b_n^{\dagger} b_m = \sum_{n} E_o\, b_n^{\dagger} b_n + \sum_{n,m}{}^{*} V_{nm}\, b_n^{\dagger} b_m \qquad (S2)$$

Here, $b_n^{\dagger}$and $b_n$ denote the Pauli operators[S1] for creation and annihilation of an excitation on molecule *n*, respectively, and the asterisk ( $^{*}$) on the last summation excludes terms with *n* = *m*. The dipolar excitation-transfer interaction in point-dipole approximation is expressed as

$$V_{nm} = \frac{1}{4\pi\varepsilon\varepsilon_0} \frac{(\vec{\mu}_n \cdot \vec{\mu}_m)|\vec{r}_{nm}|^2 - 3(\vec{\mu}_n \cdot \vec{r}_{nm})(\vec{\mu}_m \cdot \vec{r}_{nm})}{|\vec{r}_{nm}|^5} \qquad (S3)$$

where $\vec{\mu}_{n(m)}$ denotes the transition-dipole moment of molecule *n (m)*; $\vec{r}_{n(m)}$ the position of molecule *n (m)*, $\vec{r}_{nm} = \vec{r}_m - \vec{r}_n$ , and ε the dielectric constant for which $\varepsilon$ = *1* has been used. We restrict ourselves to linear optical properties and consider only one-exciton states, i.e., excited states with in total one excitation quantum. In that case, diagonalization of the $N \times N$ Hamiltonian matrix $H_{nm}$ (with $N = N_1 N_2$) yields as eigenvalues the exciton energies $E_k$, while the corresponding eigenvectors $\{a_{k,n}\}$ (normalized to unity) define the exciton wave functions expressed in the site basis:

$$|k\rangle = \sum_{n} a_{k,n} |n\rangle \qquad (S4)$$

Here, $|n\rangle$ represents the state where molecule *n* is in the excited state and all other molecules are in the ground state. The transition dipole from the total ground state (the state in which all molecules are in their ground state) to the exciton state $|k\rangle$ is

$$\vec{\mu}_k = \sum_{n} a_{k,n} \vec{\mu}_n \qquad (S5)$$

This allows us to express the polarization resolved fluorescence excitation spectrum of the aggregate (which is assumed to equal the absorption spectrum) as

$$F(E,\theta) = \frac{1}{\pi} \sum_{k} |\vec{\mu}_k \cdot \vec{e}|^2 \frac{2W_k}{4(E - E_k)^2 + (W_k)^2}$$

$$= \sum_{k} \frac{|\vec{\mu}_k|^2}{\pi} [\cos(\theta - \phi_k)]^2 \frac{2W_k}{4(E - E_k)^2 + (W_k)^2} \qquad (S6)$$

where $\vec{e}$ is the polarization vector, *E* is the energy and $\theta$ is the polarization of the excitation/incident light. $\phi_k$ is the angle of the projection of the transition dipole vector of the exciton state $|k\rangle$ relative to the laboratory frame. Given the tubular symmetry of the monomer

arrangement, only a few exciton states with their transition-dipole moments either parallel or perpendicular to the tubular axis have a finite, non-zero oscillator strength. $W_k$ is the width of the Lorentzian that is used to convolute with the spectral components with parallel and perpendicular polarization.

We connect the results from the simulations with the experimental spectra by assigning all simulated exciton states with their transition-dipole moments parallel to the tubular axis to the experimentally observed low-energy band (spectral component 1), and those with their transition dipole moments perpendicular to the tubular axis to the experimental high-energy band (spectral component 2).

**6. Scanning Transmission Electron Microscopy (STEM) of ZnChl aggregates**

STEM images as shown in fig.S8 were recorded using a Zeiss Ultra Plus field emission scanning electron microscope equipped with GEMINI e-Beam column operated at 20 kV. A drop of sample solution ZnChl in water/methanol (100:1; vol/vol) was placed on 200-mesh formvar copper grids coated with carbon. About 1 min after the deposition, the grid was tapped with filter paper to remove the remaining solution and dried at vacuum of airlock chamber.

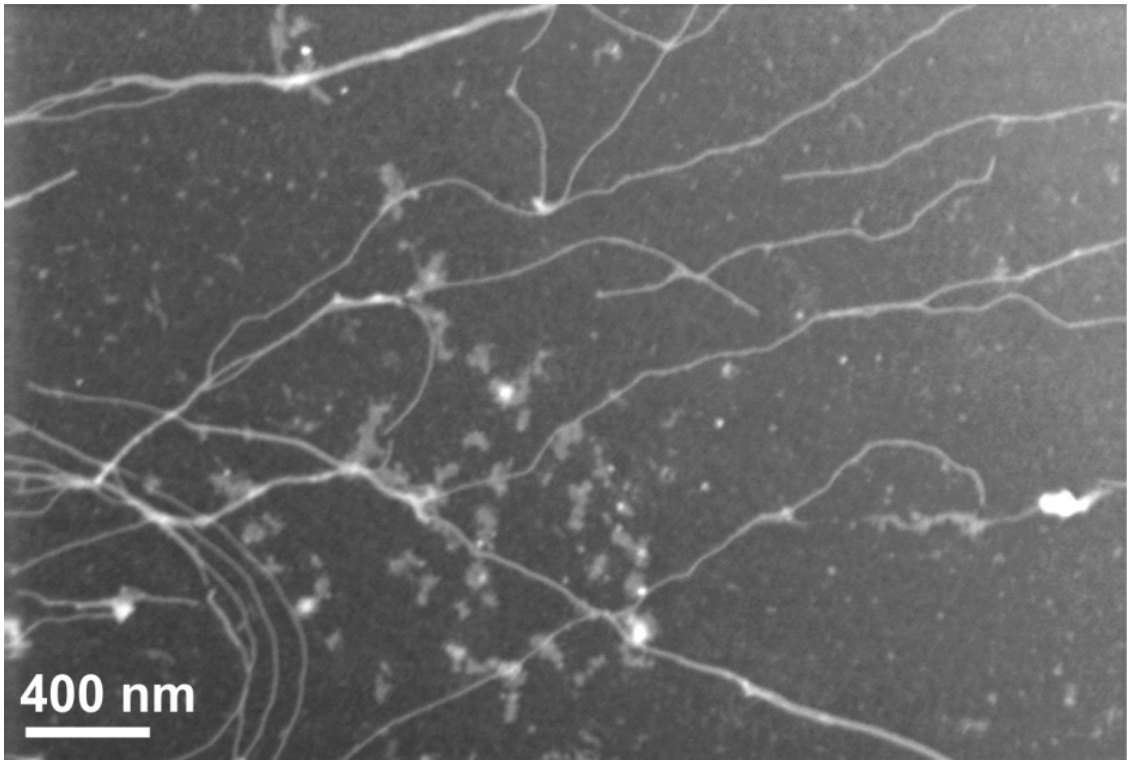


*Fig.S8:. Dark field STEM micrograph of ZnChl aggregates in water/methanol (100:1) solution at accelerating voltages of 20 kV. The long isolated nanofibers with the average diameter of about 6 nm were observed. The concentration was c = 1.0 × $10^{-5}$ M.*

**7. Optical selection of single tubules**

The selection of a single nanotube for the optical experiments took place in two steps. First the sample was excited at 735 nm. The excitation light passed a home-built microscope that was operated in widefield mode by inserting a lens into the excitation path for defocusing the laser to an area of about 30 × 30 $\mu m^2$. In order to excite the aggregates independently from their spatial orientation in the sample plane, the excitation light passed a λ/4 plate (Thorlabs Inc.) to achieve circular polarized light. The emission from the single complexes was collected by a microscope objective (Mikrothek, NA = 0.85) mounted inside the cryostat, transmitted through two long-pass filters (LP780, AHF Analysetechnik), and detected with a CCD-camera (iKon, Andor). This step served for locating the individual tubes, see fig.S9.

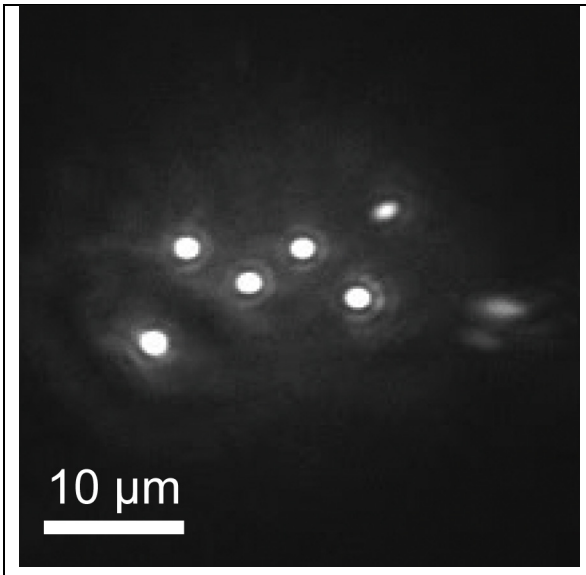


*Fig.S9: Widefield fluorescence image (epiflourescence) of several individual ZnChl **1** nanotubes. The actual size of the nanotubes cannot be resolved optically due to the diffraction of light.*

Subsequently, a well separated aggregate was selected from the widefield-image and the microscope was converted to confocal mode by removing the defocussing lens from the excitation path such that the excitation volume coincided with one of the tubes observed with the CCD camera. In this mode the excitation light is focussed to a diffraction-limited spot of about 450 nm in size. Furthermore, the λ/4 plate was replaced by a λ/2 plate (Thorlabs Inc.) providing linearly polarized light. The polarization-resolved fluorescence-excitation spectra were obtained by varying the excitation wavelength between 717 nm and 750 nm by rotating a birefringent filter with a stepper motor (Actuator 850F, Motion Controller MM4005, Newport) in the cavity of the Titan-Sapphire-laser (3900S, Spectra Physics). The reproducibility and accuracy of the excitation wavelength was measured with a wavemeter (WaveMaster, Coherent) and amounts to 1 $cm^{-1}$. Between two successive laser scans the polarization of the excitation light was rotated by 6.2° by turning the $\lambda$/2-waveplate with a stepper motor (Owis GmbH). The emitted light from the complexes passed the two long-pass filters

mentioned above and was detected with a single-photon counting avalanche photodiode (APD) (SPCM-AQR-16, Perkin Elmer). During each experiment, a fraction of the excitation light was split off and registered as a function of the wavelength by a powermeter (LaserMate-Q, Coherent). This was used for correcting spectral variations of the excitation intensity. The excitation intensity was 25 W/cm$^2$, and all experiments were conducted at 1.2 K. A similar setup is described in great detail in Refs.[2,3]

References SI:


(1) Davydov A. S. *Theory of Molecular Excitons*; Plenum Press: New York, 1971.

(2) Hofmann, C., Aartsma, T. J., Michel, H., Köhler, J. Spectral dynamics in the B800 band of LH2 from Rhodospirillum molischianum. A single-molecule study. *New J. Phys.* **2004**, *6*, 8 - 15.

(3) Lang, E., Baier, J., Köhler, J. Epifluorescence, confocal and total internal reflection microscopy for single-molecule experiments: a quantitative comparison. *J. Microsc.* **2006**, *222***,** 118–123.